

PROJECT DESCRIPTION: III: Small: Reconstruction and Analysis of the Full Vascular Network of the Mouse Brain

A. Introduction

Goal: The long-term goal of this project is to design and develop an informatics platform for a detailed quantitative investigation of geometrically complex biological data from whole animal organs.

Target Data Set and Its Scientific Value: This project will focus on whole mouse brain blood vessel (vasculature) data [21, 55] obtained using a unique instrument we developed, the Knife-Edge Scanning Microscope (KESM) [51, 58, 61]. The KESM (Fig. 1), a physical sectioning 3D microscope, (1) gives data that have an unprecedented amount and scale: several terabytes of data per organ at the scale of the whole organ ($\sim 1 \text{ cm}^3$ in volume), down to the smallest capillaries (3 to 4 μm in diameter in rodents [72]). (2) KESM has very high data acquisition rate (<100 hours per organ, orders of magnitude faster than competing approaches), and (3) enables the investigation of highly complex biological organizations (fractal-like network) [18, 24].

Such a data set addresses a key gap in brain vasculature data since most existing data sets either have orders of magnitude lower resolution than the KESM or do not have full organ coverage. For example, magnetic-resonance-based spiral imaging can capture blood vessels in whole organs but has the resolution of $78\mu\text{m} \times 78\mu\text{m} \times 500\mu\text{m}$ [48], which is not enough to resolve the finest capillaries (3 to 4 μm in diameter). X-ray synchrotron tomography can go down to 1.4 μm resolution but the imaging volume is limited to about 3 mm in linear dimension [72]. In terms of the brain, the current efforts using high-resolution microscopy to image the brain vascular system are mostly focused on the cortex [10, 16, 17], leaving out major subcortical nuclei such as the thalamus and basal ganglia; and the cerebellum. Moreover, informatics platforms do not exist for such data sets for quantitative analysis, although there are recent efforts in quantitative modeling and analysis of the vascular networks [16, 17, 42] and their development over time [7, 41, 47, 78, 80]. In our project, we aim to fill this critical gap: (1) lack of data and (2) lack of an informatics platform.

The resulting data and informatics platform are expected to have significant scientific impact. The KESM mouse brain vasculature data set can help address major scientific questions such as oxygen and nutrition transport in the brain [30, 31]; redundancy and robustness of biological networks [10]; and neurophysiological correlates of brain activation (e.g., blood-oxygen level dependent signals as a proxy of neuronal activity [11, 76]; see [14] for the correlation between capillary loss and cognitive deficits). Furthermore, organizational principles drawn from the vascular network data can help engineer robust distribution networks (e.g., using scaffolding methods reported in [67]), resilient computer networks, and fail-safe power grids (see the discussion in [10] and discussion of networks in general in [4]). For example, [10] showed that the vascular network near the pial surface of the rodent brain has Kirchhoff-like loops that allow robust distribution of blood. Finally, a detailed map of the vascular network can be used to design deep-brain stimulation probes that use the vascular network as a conduit, rather than electrodes that damage brain tissue upon insertion.

Objectives: The main objectives of this project are as follows (corresponding to §C.1–§C.6):

1. KESM mouse brain vascular data acquisition (additional data), and image processing and registration.
2. Development of fast and robust automated reconstruction algorithms to recover the full geometry of the mouse brain vascular network.

3. Development of a model-based vascular network generator.
4. Development of a model-based validation system.
5. Development of a Scalable Vector Graphics(SVG)-based web informatics platform.
6. Inferring the optimization principles of the whole mouse brain vascular network development and organization using the informatics platform.

Summary of Intellectual Merit and Broader Impacts: Please refer to the project summary.

B. Background and Prior Work

B.1. Physical Sectioning Microscopy for Volume Imaging

Critical to our proposed work are massive biological data sets sampled at sub-cellular resolution to which our computation will be applied. The technologies for producing such massive data are actively being developed. Examples of such methods include our Knife-Edge Scanning Microscopy (KESM) [51, 58, 59, 60, 61] (see §B.2), All-Optical Histology [85], Array Tomography [65], Serial-Block-Face Scanning Electron Microscopy (SBF-SEM) [26], Automatic Tape-Collecting Lathe Ultramicrotome (ATLUM) [36, 37], and the most recent Serial Two-Photon Tomography [74]. Unlike Array Tomography and SBF-SEM, KESM can survey large volumes of biological tissue (whole small animal organs), and KESM is an order of magnitude faster than All-Optical Histology, ATLUM, and Serial Two-Photon Tomography. SBF-SEM has the advantage of ultra high resolution, and Array Tomography is ideal for repeated imaging of a single specimen with multiple immuno stains. Table 1 below shows a summary comparison of the above approaches.

Table 1: Comparison of KESM and Related 3D Microscopy Technology.

| Method | High-Resolution | High-Volume | High-Throughput |
|-----------------------------------|-----------------|-------------|-----------------|
| KESM [51] (cf. [49]) | ✓ | ✓ | ✓ |
| All-Optical Hist. [85] | ✓ | ✓ | — |
| Serial Two-Photon Tomography [74] | ✓ | ✓ | — |
| Array Tomography [65] | ✓ | — | — |
| SBF-SEM [26] | ✓ | — | — |
| ATLUM [37] | ✓ | ✓ | — |
| X-ray synchrotron tomography [72] | ✓ | — | — |
| MRI/diffusion MRI [33, 40] | — | ✓ | ✓ |

High-resolution: $\sim 1 \mu\text{m}$ (diameter of dendrites, axons, capillaries, etc.); High-Volume: $> 1 \text{ cm}^3$ (approximate volume of mouse brain and other organs); High-Throughput: < 100 hours (for ~ 50 scanned organs per year).

B.2. Imaging with the Knife-Edge Scanning Microscope

A prototype Knife-Edge Scanning Microscope (KESM, US patent #6,744,572) [58, 59, 61] has been designed at Texas A&M University (TAMU) with support from the National Science Foundation (MRI award #0079874; McCormick, PI), the Texas Higher Education Coordinating Board (ATP award #000512-0146-2001; Keyser, PI), and the National Institute of Neurological Disorders and Stroke (Award #1R01-NS54252; Choe, PI). The instrument, shown in Fig. 1a, is capable of scanning a complete mouse brain ($\sim 310 \text{ mm}^3$) at 300 nm sampling resolution within 100 hours when scanning in full production mode. The major components of the instrument are shown in the figure and explained in the caption. Fig. 1b illustrates the imaging principle. A custom diamond knife, rigidly mounted to a massive granite bridge overhanging the three-axis stage, cuts consecutive thin sections from the block. Unlike block face scanning, the KESM concurrently cuts and images (under water) the tissue ribbon as it advances over the leading edge of the diamond knife. A white light source illuminates the rear of the diamond knife, and in turn illuminates the brain tissue at

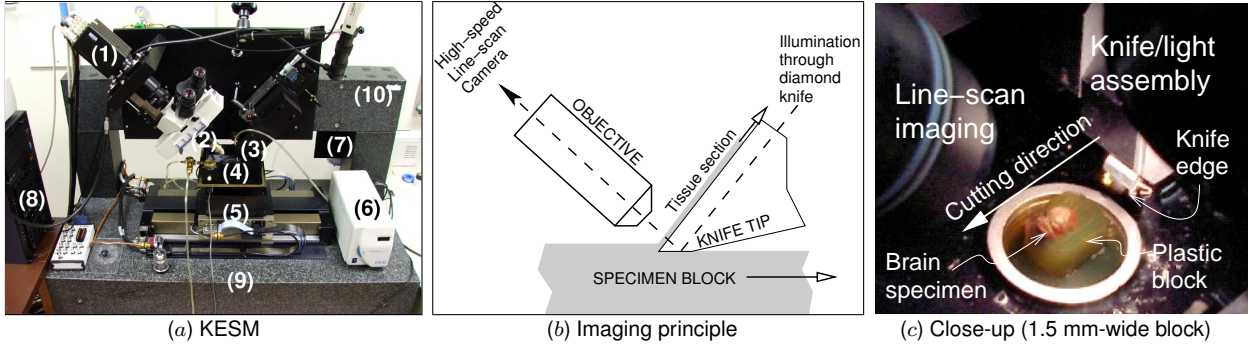


Figure 1: The Knife-Edge Scanning Microscope (KESM). (a) Photo of the KESM showing (1) high-speed line-scan camera, (2) microscope objective, (3) diamond knife assembly and light collimator, (4) specimen tank (for water immersion imaging), (5) three-axis precision air-bearing stage, (6) white-light microscope illuminator, (7) water pump (in the back) for the removal of sectioned tissue, (8) PC server for stage control and image acquisition, (9) granite base, and (10) granite bridge. (b) Specimen undergoing sectioning by knife-edge scanner (thickness of section is not drawn to scale). (c) Close-up photo of the line-scan/microscope assembly and the knife/illumination (knife and objective raised to show the brain specimen).

its leading edge, with a strip of intense illumination reflected from the beveled knife-edge. The microscope objective, aligned perpendicular to the top facet of the knife, images the transmitted light. A high-sensitivity line-scan camera continually samples only the newly cut portion of the tissue ribbon right at the very tip of the knife edge, prior to any subsequent deformation of the tissue as the ribbon slides up the knife. Finally, the successive line images are passed through image acquisition boards and stored in a dedicated cluster computing system.

B.3. Imaging results using KESM

Fig. 2 shows our mouse brain vascular network data set (India ink stained) [21, 22, 55]. India ink stains all blood vessels in the tissue sample. Major arteries and veins down to the smallest capillaries are stained, revealing a complex network. The smallest capillaries are around 3 to 4 μm in diameter [72], which corresponds to 3 to 4 voxels in our data set.

B.4. Rapid tracing of fibrous matter

In order to turn the raw data into a geometric description of the objects of interest (i.e., reconstruction), we are currently developing rapid tracing algorithms for fibrous matter such as neuronal processes and neurovasculature [18, 50, 53, 57]. Fig. 3 shows an overview of our approach, which is broadly classified as a vector tracing method [2, 15]. Our method has been used successfully on KESM and Array Tomography data. See Fig. 3d for preliminary results.

B.5. Web-based light-weight 3D brain atlas

We have taken initial steps in making available, over the internet, the massive volume image stack from KESM (<http://kesm.org>). The multi-scale 3D rendering brain atlas only requires a standard web browser without any add-on or plug-in (thus “light-weight”). The basic idea is to use image overlays with distance attenuation for 3D rendering. See [24, 27] and Fig. 11a&b for details.

B.6. Results from prior NSF support

The results from prior NSF support in the past five years are summarized below. (1) NSF CRCNS data sharing #0905041: PI: Choe, Co-PIs: Abbott, Keyser; \$114,024 (09/01/2009–12/31/2011); Title: CRCNS data sharing: Whole Mouse Brain Neuronal Morphology and Neurovasculature Browser. (2) NSF CRCNS #1208174: PI: Choe, Co-PIs: Abbott, Keyser; \$200,868 (09/01/2012–08/31/2014); Title: CRCNS: Data Sharing: Open Web Atlas for High-Resolution 3D Mouse Brain

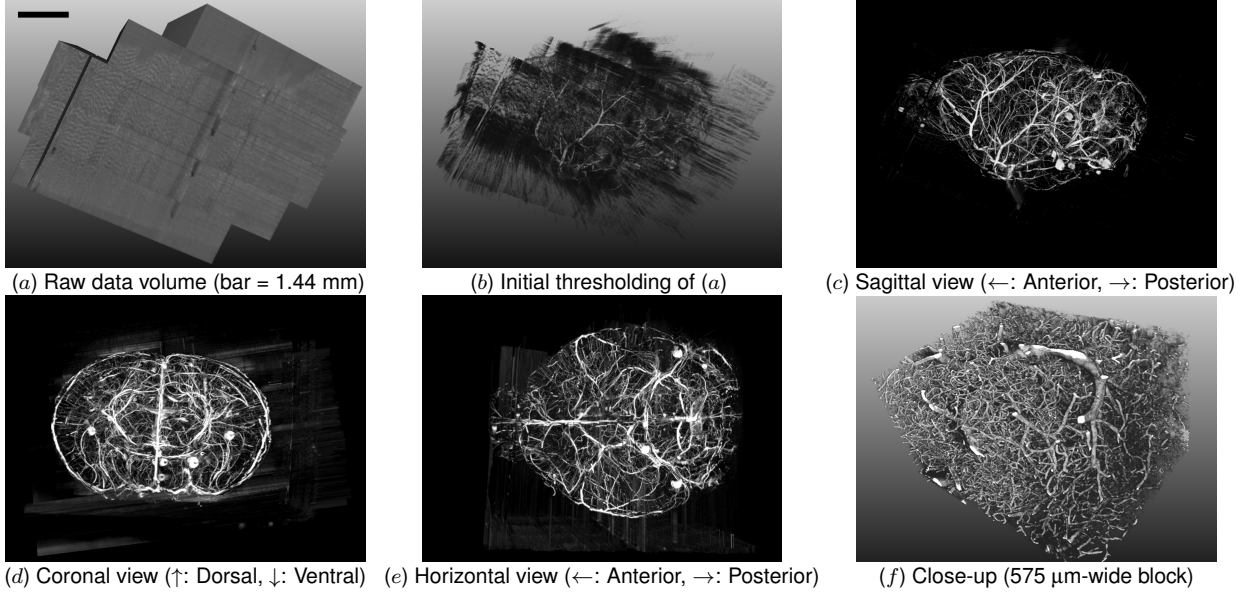


Figure 2: KESM Mouse Brain Vasculature Data. Various views/scale of the KESM vasculature data are shown: (a) a raw data block in a sagittal view (scale bar = 1.44 mm). Five tilted image stacks can be seen (top of each stack facing the upper-left corner). (b) A mildly thresholded version of (a). The boundary of the data block and the content within can be seen in context. (c) A fully thresholded version of (b). (d)–(e) The coronal and horizontal views of (c), respectively. We can clearly see the shape of the brain. (f) Intricate details in a 575 μm -wide block (0.6 μm \times 0.7 μm \times 1.0 μm voxel resolution).

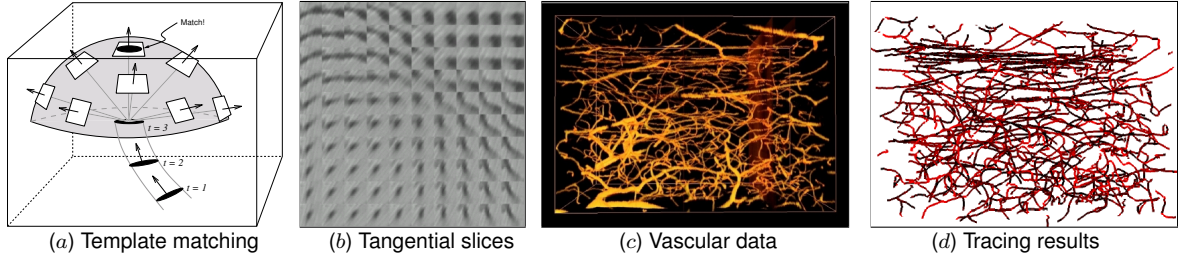


Figure 3: Fast Fiber Tracing. The basic idea behind our fast fiber tracing algorithm is shown. (a) Starting from a seed point ($t = 1$), the direction of the fiber is estimated ($t = 2$ to $t = 3$). The next point in the fiber trajectory is estimated using a template-based approach. Images are formed as interpolated slices (computed via graphics hardware) through the data volume—sampling in several directions around the current point. (Note that the distance between trace points is exaggerated.) (b) A typical array of slices from the tangential planes are shown. Only a small number of these resemble a circular cross-section of a fiber (upper-right corner). The best matching one is selected as the next point in the fiber trajectory. (c) Volume rendering of cortical vasculatures are shown (width = 350 μm). (d) Tracing results on (c) are shown. (Pilot results presented in [53].)

Data. (Co-PI Keyser was also funded by NSF grant #0917286, but it was on a relatively unrelated topic so we will not discuss it in detail here; see these selected publications resulting from the project: [8, 9, 38, 92].) The outcomes from the above projects were as follows: (1) **Publications:** 3 journal papers: Frontiers in Neuroinformatics [24], Biomedical Optics Express [55], Journal of Visualized Experiments [23]; 3 conference papers: [22, 44, 54]; 2 abstracts: [19, 20]. (2) **Data:** The web-based KESM Brain Atlas (<http://kesm.org>), online since September 2012, is serving ~4.5 Teravoxels of data from two Golgi-stained mouse brains (neuronal morphology) and one India-ink-stained mouse brain (vasculature). We have also made our atlasing code available to the public on SourceForge (project “kesmba”). (3) **Broader Impacts:** Graduate students trained (3 students): Chul Sung, Daniel Miller, Jinho Choi (one directly funded by this grant); Undergraduate

students trained (2 students): Aaron Panchal (coauthor of [54]), Jonathan Garcia (now with the UCSD neuroscience graduate program); Exhibits at conferences (3 times): International Joint Conference on Neural Networks (2011), Society for Neuroscience (2011, 2012); Lab tours to the public (2 times): Aggieland Saturday (2012), USA Science and Engineering Festival (2010).

New in the proposed project: Our previous projects were based on raw image stacks that did not include any geometric reconstruction, thus quantitative investigation was not supported. Furthermore, the previous projects focused on the neuronal network, not on the vascular network. In the current project, we focus on informatics based on fully reconstructed and validated geometric reconstructions of the mouse brain vascular network.

C. Research Plan

We will acquire mouse brain vasculature data, reconstruct the geometry, validate the results (using digital phantoms [71]), and build an informatics platform to infer organizational optimization principles. Our project will be carried out in three main phases, roughly corresponding to one phase per year:

- Phase 1, data acquisition and reconstruction: §C.1 will outline the data acquisition and image processing steps; §C.2 will give our detailed plan for automated reconstruction.
- Phase 2, vascular network model and model-based validation: §C.3 will provide details on how to generate statistically accurate and realistic vascular networks; §C.4 will explain in detail how validation will be done based on the model-based ground truth.
- Phase 3, informatics platform: §C.5 will discuss the design of an SVG-based informatics platform; §C.6 will present our plans for statistical analysis of the data.

C.1. Data acquisition and image processing/registration

C.1.1. Stain and prepare specimen

We will examine the brain of the laboratory mouse, as it offers certain advantages for study. The brain is small; its cortex is not folded; tracing experiments and imaging techniques can be performed on live mouse brain; the statistical characteristics of its microscopic features have been quantified carefully and extensively [13]; and the laboratory mouse is the leading mammalian model for genomic modeling and gene modification experiments. C57BL/6J mice have been chosen as representatives of the mammalian brain as they are a very common inbred mouse strain used for transgenic studies and aging research. Mice for this study will be obtained from an on-campus source through Co-PI Louise Abbott. Brains from four mice will be used. Note that part of the brain specimen (one brain) will be used for pilot runs of the KESM, thus those particular data may not be stored for analysis. Data from three mice will be collected and analyzed for the production runs. We will use India ink to stain the vascular network in the mouse brain. The mice are perfused transcardially with saline, then 10% formalin and finally with India ink, which fills the cardiovascular system. The ink stays in the blood vessels during processing of the tissue for embedding. We will perform whole body perfusions with fixatives and India ink such that the entire brain is perfused sufficiently. See [1, 23, 39, 75] for the exact protocols. After staining, the whole brains are dehydrated through a series of graded ethyl alcohols (25%–100%) followed by xylenes and then infiltrated with araldite and embedded in blocks [1, 23]. Note: although we will focus on the brain for this project, the above protocol can be applied to many other organs including the liver, kidney, and the lung.

C.1.2. Section and image with KESM

Procedures described in §B.2 will be used to generate massive volumetric data sets from each of the stained and embedded specimens described above. The prepared specimens are then

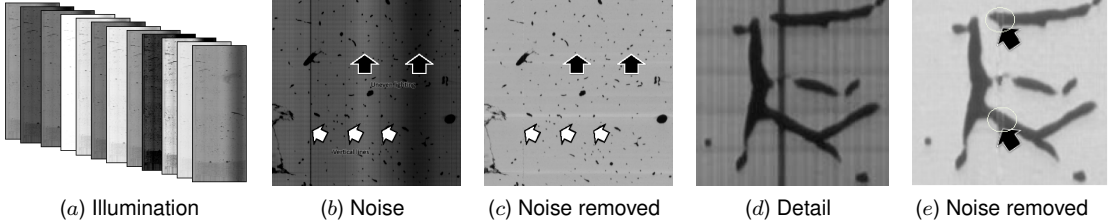


Figure 4: KESM Image Noise and Noise Removal. Various forms of KESM image noise and results of noise removal are shown. (a) Uneven illumination across images due the cutting speed variation to avoid mechanical chatter. (b) Local illumination bands (black arrows) and knife-defect bands (white arrows). (c) Noise-removed version of b. (d) Close-up of knife-defect band. (e) Noise-removed version of d using selective normalization.

scanned by the KESM using a fully automated process. The output of this scanning will be a large volumetric grid of intensity values. Each pass of the knife captures a range of x values (e.g. 2048 or 4096 pixels), across the entire y range (9,000-30,000 pixels); typical scans are $4096 \times 12,000$. Adjacent slices in x are taken in a stair-step manner in order to create a complete cross-section of the tissue. Thousands of consecutive slices are also taken in the z direction. The data produced from a scan of a single mouse brain is currently over 1.5 TB (10X, NA 0.3, Nikon objective).

C.1.3. Imaging artifact removal and image registration

Knife-edge scanning microscopy has its own sources of noise and artifacts. The primary sources of error include: misalignment of the knife edge (causing a uniform gradient to appear in the image), defects in the knife blade (causing “streaks” in the y -axis of the image), oscillations in the light source due to AC power fluctuation (causing a regular pattern of light changes along the y -axis), and knife chatter (causing horizontal lines and loss of most data at those pixels) in the image (see Fig. 4 for details).

Image registration issues are minimal due to the way KESM is designed and built: Line scan is used at the very tip of the knife as soon as the tissue comes off of the block face, thus the distortion is minimal, and successive scans in the z direction are almost exactly aligned.

We have already developed methods for automatically cleaning this data [46, 56] (Fig. 4), retrieving the data-containing region, and aligning the stacks [45]. The full algorithm is as follows: (1) Normalize pixel intensity $n(x, y)$ by row and then by column: $n(x, y) = \frac{p(x, y)}{\text{median}(\text{row}(y))} \times B$, where $p(x, y)$ is the pixel at (x, y) , $\text{median}(\cdot)$ is the median value, $\text{row}(\cdot)$ is the set of pixels in the row, and B is the desired background intensity. Column normalization is done in a similar manner. Use of B allows background illumination to become the same over all images in the image stack. (2) Apply step 1 using selective normalization, where pixels are restored to their original value when their normalized values occupy the darker-end peak region (i.e., foreground) in the intensity histogram (Fig. 4d&e). (3) Remove local artifacts due to cutting irregularities using adaptive local scaling: $p(x, y) = \frac{p(x, y)}{\text{mean}(L(x, y))}$, where $L(x, y)$ is a local window around (x, y) . (4) Crop non-data portion of the image using a boundary detection template to calculate the cut-off column $x_{\text{cutoff}} = \text{argmin}_x (\sum_{c=0}^w \sum_{r=0}^h |p(x + c, y + r) - p(x, y)|) + \frac{w}{2} - W$, where $p(x, y)$ is the pixel, (w, h) is the template width and height, and W is the width of the uncropped image. We have found that these algorithms are sufficient in removing most KESM-specific artifacts from the images. Finally, (5) we use registration using our pattern-matching-based registration algorithm described in [45].

Research issues: Although images from KESM are nearly perfectly aligned due to the design of the instrument, minor distortions are possible. In case of such distortion, we will employ local deformation-based registration methods that use Moving Least Squares (MLS, [77]).

C.2. Develop fast, robust tracing algorithms

Our goal is to extract from the KESM volume data set the individual geometric structures of interest. We have developed a series of vector-based tracing algorithms [35, 50, 52, 63]. *Here, we will discuss [35] in detail, while leaving open the option of adopting our other approaches [50, 52].*

Our maximum intensity projection(MIP)-based algorithm provides a general framework for 3D tracing, and one unique strength is that it can use any 2D tracing algorithm as a subroutine. Thus, the overall power of our MIP-based algorithm can be arbitrarily increased by the use of more powerful 2D tracing algorithms. Furthermore, our algorithm takes only about 30% of the time to trace a unit block compared to a full 3D algorithm. The algorithm consists of four steps, starting from a seed point: (1) boundary detection and local axis length determination, (2) local volume estimation and local MIP processing, (3) 2D tracing of fiber direction, and (4) 3D fiber direction estimation and adjustment. Fig. 5c shows an overview of our approach (for details see [35]).

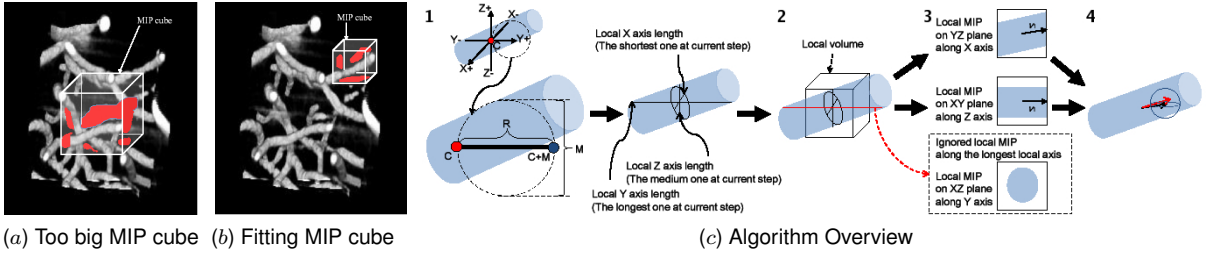


Figure 5: Vector Tracing with Local Maximum-Intensity Projection (MIP). (a-b) Local MIP size has to be small enough for unambiguous, occlusion-free projection (a contains occlusions while b does not). (c) The local MIP-based tracing algorithm is outlined. 1. Starting from seedpoint C, longest-axis boundary C+M is found and the boundaries along the other two axes are found. 2. Local MIP cube size is determined. 3. 2D trace is conducted on two of the three MIPs. 4. Results are combined in 3D.

(1) First, we define $P_{in}(\vec{c}, R)$, $P_{out}(\vec{c}, R)$, and $P_{edge}(\vec{c}, \tau)$ as the probability of a voxel R-voxels (or τ -voxels) apart from the trace center \vec{c} being inside, outside, or on the edge of the fiber, respectively (Gaussian functions are used). From this, we obtain the edge map $E(\vec{c}, R, \tau) = \frac{1}{3}(P_{in}(\vec{c}, R - \tau) + P_{out}(\vec{c}, R + \tau) + P_{edge}(\vec{c}, \tau))$, and $E(\vec{c}, R) = \max E(\vec{c}, R, \tau)$. The foreground-background boundary along the three axes x , y , and z are found by calculating $\text{argmax}_{R \in [\vec{c}, \dots, \vec{c} + M\vec{e}]} E(\vec{c}, R)$ where M is the maximum fiber width and \vec{e} is the unit vector along one of the principal axes. (2) From these boundaries, the local MIP volume is created, and MIPs are generated on the XY, YZ, and XZ planes. Among these, the projection along the longest fiber direction is ignored since it does not contain fiber direction information. (3) Tracing in 2D is done using a multiscale filter using a Hessian matrix $H_\sigma(x) = \begin{bmatrix} I_{xx}(x) & I_{xy}(x) \\ I_{yx}(x) & I_{yy}(x) \end{bmatrix}$, where $I_{uv}(x) = \sigma^2 \frac{\partial^2 G(x, \sigma) I(x)}{\partial u \partial v}$, where σ is the scale, and $G(x, \sigma)$ is a Gaussian with standard deviation σ , and $I(x)$ is the voxel x in the data volume I . The eigenvector \vec{v}_1 corresponding to the smallest eigenvalue λ_1 indicates the fiber direction. To elaborate, first a fiber-likeness function $V(x, \sigma)$ is defined as 0 when 2nd eigenvalue $\lambda_2 > 0$, and as $\exp\left(-\frac{\lambda_r^2}{2\beta^2}\right) \left(1 - \exp\left(-\frac{S^2}{2c^2}\right)\right)$ otherwise, where $\lambda_r = \frac{\lambda_1}{\lambda_2}$, and $S = \sqrt{\sum_{i=1}^2 \lambda_i^2}$, and β and c control the sensitivity of the Hessian filter (0.5 and 0.25, in our experiments). The maximum value along $V(x, \sigma)$ at scale σ gives the eigenvector \vec{v}_1 , which is the fiber direction (see [29] for details). (4) Finally, from the 2D tracing on the two MIP planes, the 3D fiber direction is estimated as follows. Assume that XY and YZ were the two chosen planes. Let $\vec{v}_{xy} = (x_1, y_1, 0)$ and $\vec{v}_{yz} = (0, y_2, z_2)$ be the eigenvectors from the two respective MIP planes. The 3D fiber direction is derived as $\vec{v}_{xyz} = (x_1, \frac{y_1+y_2}{2}, z_2)$. From this, the next trace center \vec{c}' can be calculated as $\vec{c}' = \frac{\vec{v}_{xyz}}{\|\vec{v}_{xyz}\|} \rho + \vec{c}$, where ρ is the step size (currently set to 3). The last step corrects for discretization error where we

use a momentum operator to calculate the adjusted center $(\bar{x}, \bar{y}, \bar{z}) = \left(\frac{M_{100}}{M_{000}}, \frac{M_{010}}{M_{000}}, \frac{M_{001}}{M_{000}} \right)$, where $M_{pqr} = \int_z \int_y \int_x x^p y^q z^r I(x, y, z) dx dy dz$ (see [12] for details).

Our algorithm, due to the use of a 2D Hessian matrix, has computational complexity of $O(n^2)$, while full 3D tracing algorithms based on 3D Hessian matrices have $O(n^3)$ complexity, where n is the scale of the Gaussian filter. In practice, our algorithm takes only about 30% of the time of full 3D versions. Initial implementation of this and related approaches has proven successful [35, 50, 52, 63], and we will modify and improve it to trace a wider variety of fibrous data.

Research issues: It is possible that the calculation of the Hessian matrix can become incorrect due to noise in the data or misalignment of images in the image stack. However, smoothing with a multi-scale Gaussian kernel ($G(x, \sigma)$) eliminates most of the noise, and the registration issue does not arise due to the design of the KESM. Furthermore, if this turns out to be a problem, we will adopt techniques such as directional decomposition to overcome the shortcoming [43].

C.3. Develop a model-based vascular network generator

We will develop a model-based vascular network generator to serve two purposes: (1) to generate synthetic data for the validation (§C.4) of our automated reconstruction algorithm (§C.2), and (2) to infer organizational optimization principles (§C.6).

Our vascular network generator will be based on two processes observed in biology: (1) vasculogenesis, the generation of blood vessels from scattered endothelial cells that self-organize into capillary networks [69, 80], and (2) angiogenesis, sprouting of new vessels from existing vessel segments [3, 84]. Developmentally, vasculogenesis precedes angiogenesis, thus our vascular network generator will run in two stages.

Vasculogenesis model: Our vasculogenesis model will be based on that of Serini et al. [80]. The cell population (cell position \vec{x}) will be modeled as a distribution with local cell density n and velocity \vec{v} that depends on the cell's position. Chemoattractant concentration c will control the growth. The model is governed by the following equations. First, conservation of mass is enforced by $\frac{\partial n}{\partial t} + \nabla \cdot (n\vec{v}) = 0$, where t is time. Next, the momentum and chemotactic forces are balanced using $\frac{\partial \vec{v}}{\partial t} + \vec{v} \cdot \nabla \vec{v} = \beta \nabla c$, where β determines the strength of cell response. Finally, the chemoreactant generated by the endothelial cells is modeled as $\frac{\partial c}{\partial t} = D\delta c + \alpha n - \tau^{-1}c$, where D is the diffusion coefficient, α is the release rate, and τ is the degradation time. Fig.6 shows experimental observation compared to the model, both reported in Serini et al. [80].

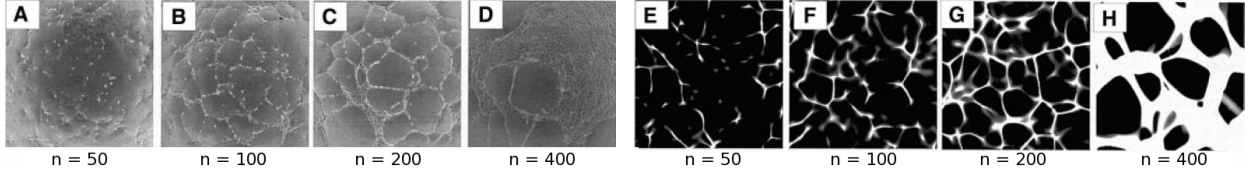


Figure 6: Serini et al.'s Vasculogenesis Model. Experimental data (A–D) and model results (E–H) reported by Serini et al. [80] are shown (n indicates local endothelial cell density).

Angiogenesis model: Our angiogenesis model will be based on that of Cassot et al. [16]. Fig. 7 provides the terminology and an outline of the branching and growth algorithm [34]. Please see Fig. 7 caption for the definition of “segment”, “element”, and “order”.

1. Initialization: generate an element of a given order, say n and $n - 1$ (usually a high value, greater than 3; Fig. 7b, Left). Daughter elements are sprouted off from this initial element down to order 0 elements (terminal tips).
2. Branch generation in initial vasculature: Using statistics from the ground truth, generate branches at specific locations of the segment (Fig. 7b, Right).

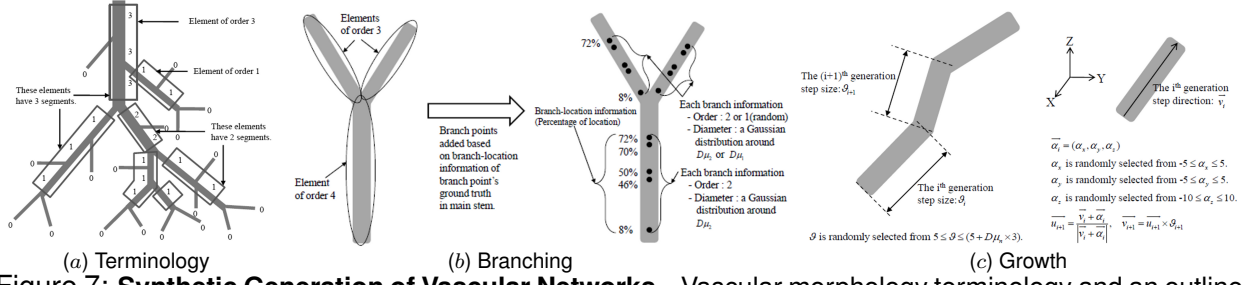


Figure 7: Synthetic Generation of Vascular Networks. Vascular morphology terminology and an outline of the synthetic vascular network generation procedure are shown. (a) A “segment” is an intact piece of vasculature between branch (or terminal) points. A series of segments that belong to the same trunk is called an “element”. Each element has a numerical “order”, which is how far they are from the terminal tip in terms of the number of branches. (b) Procedure for sprouting new branches on existing elements is shown. (c) Procedure for the growth of existing elements is shown. See [34] for details.

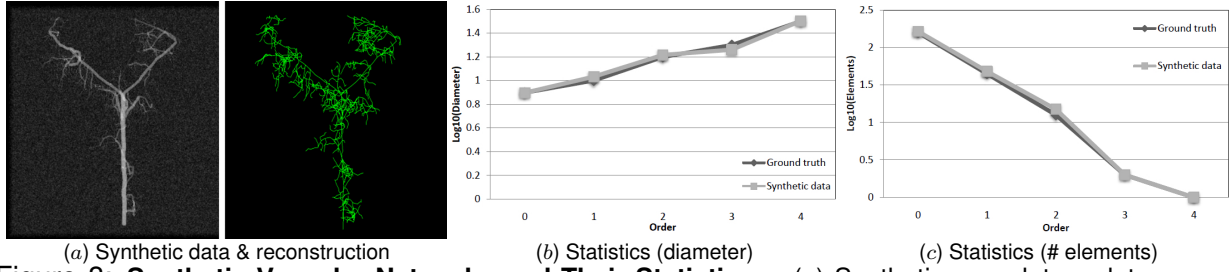


Figure 8: Synthetic Vascular Networks and Their Statistics. (a) Synthetic vasculature data, reconstruction, and (b–c) morphometric statistics are shown. The diameter and number of element distributions are a close match with the ground truth (pilot results reported in [34]).

3. Grow elements: Determine the step size (growth amount) and step direction (direction of growth) as shown in Fig. 7c and grow the elements accordingly.
4. Repeat steps 2–3 recursively for lower order elements.

Synthetic data generation and statistical validation: We will use the vasculogenesis and the angiogenesis algorithms to generate synthetic vascular networks. For morphological parameter estimation, we will gather element diameter, length, and the segment/element count grouped by the order. Full distributions will be gathered from a manually validated geometric reconstruction from KESM data, to be compared with those calculated from the synthetically generated vascular networks. Fig. 8 shows pilot results from our implementation of the algorithm and statistical validation. The figure also shows our reconstruction of the synthetic vascular network.

Research issues: The immediate problem is how to integrate the initial vasculogenesis stage and the subsequent angiogenesis stage. This could be solved by taking a multi-scale approach. We can generate an initial network using the vasculogenesis approach at a small scale and linearly scale the network to a larger volume. Then, we can use this vascular network for initialization of the angiogenesis algorithm (step 1). Our KESM vasculature data set is inherently multi-scale, thus a subsampled version (Fig. 2c–e) can be used to match the initial vasculogenesis stage, and the full resolution version (Fig. 2f) to match the angiogenesis stage. Another issue we need to overcome is the prevalence of loops in the vascular network topology, especially near the arteriole–venule interface [41] and on the pial surface of the cortex [10]. We will begin with proximity-based merging of terminal tips (order 0 elements). Existing vasculogenesis models assume a 2D substrate. We expect to be able to extend Serini et al.[80]’s approach into 3D without much trouble. Finally, to increase the fidelity of our synthetic data, we will consider measures such as branch angle, asymmetry index, and other morphometric features in addition to length, diameter, and count.

C.4. Develop a model-based validation system

We will develop a large-scale validation framework where a recursive, iterative improvement of the reconstruction algorithm and the validation procedure are interlocked together. Validation is an important necessary step in any automated reconstruction system [71, 89, 91]. A complete validation would require manually reconstructed ground truth, so it is not practical. Here, we focus on validation based on selective sampling and digital phantoms (see [71] for a review on the use of digital phantoms). We will develop our validation approach in two stages. In the first stage, we will use small volumes of data, performing validation over these volumes. Then in the second stage, we will scale up the validation to large-scale volumes. Both stages will use an iterative improvement process to improve our reconstruction approach. The reconstruction algorithm and the digital phantom function will be co-learned using an Expectation-Maximization framework [62], through a recursive improvement process. We will repeatedly refine our reconstruction and digital phantom algorithms to improve on the given metrics.

C.4.1. Selective small-scale validation

As a first step, we will operate on small volumes of data, for example, a $300\mu\text{m} \times 300\mu\text{m} \times 300\mu\text{m}$ cube of mouse brain. Consider Fig. 9 which illustrates the image acquisition and reconstruction process. Given the data volume (image stack I) obtained from KESM, we will have domain experts (from Co-PI Abbott's lab) label the data to provide the ground truth \hat{M}_e (note that the domain expert's morphological labeling is in itself an estimation of the actual ground truth M).

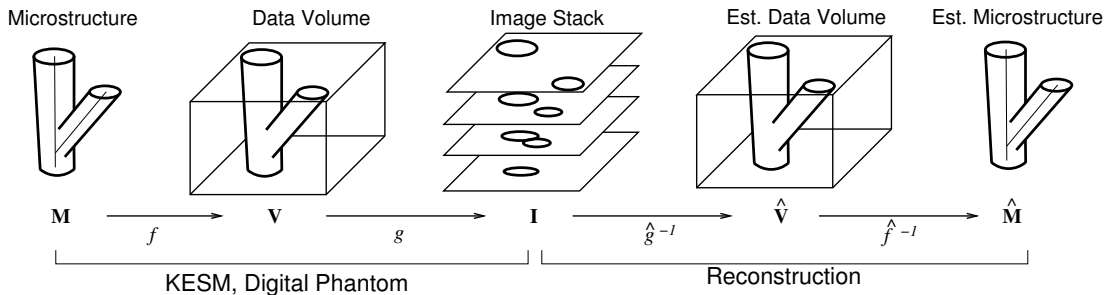


Figure 9: Microstructure-to-image Mapping and Reconstruction. The process by which a microstructure (real or synthetically generated) is turned into a stack of images in KESM and how they are reconstructed is shown. Modeling this process ($g \circ f$, composition of g and f) enables the generation of realistic synthetic image data (digital phantoms). On the other hand, the task of recovering the structural descriptions from the image data is basically the inverse: $\hat{f}^{-1} \circ \hat{g}^{-1}$, a composition of the segmentation (\hat{g}^{-1}) and the 3D reconstruction process (\hat{f}^{-1}). (The “ $\hat{\cdot}$ ” symbol indicates that these functions are estimates.) Validation can take three approaches: (1) given I from KESM and \hat{M}_e from human labeling, generate reconstruction \hat{M} from I and compare it with M_e , (2) given a digital phantom I with ground truth M , reconstruct \hat{M} from I and compare it with M , or (3) Given I and its reconstruction \hat{M} , use the mapping $g \circ f$ to create \hat{I} and show the difference image $\hat{I} - I$ that can be accepted or rejected.

Concurrently with manual labeling, the data volume I will be put through our segmentation and reconstruction algorithms, producing the estimated microstructure \hat{M} . Validation can now be done by comparing \hat{M}_e (by the domain expert) and \hat{M} (by the reconstruction algorithm). We will use mutual information for the comparison: $I(\hat{M}_e, \hat{M}) = H(\hat{M}_e) + H(\hat{M}) - H(\hat{M}_e, \hat{M})$, where $H(\cdot)$ is the Shannon entropy $-\sum_{p \in P} p \log p$, and $H(\cdot, \cdot)$ the joint entropy. We will also employ measures such as normalized mutual information, entropy correlation coefficient, and gradient [73].

The key research issue in this task is how to map corresponding parts in the geometric microstructure model of the ground truth \hat{M}_e to that of the estimate \hat{M} in order to estimate the joint probability. We will employ two approaches. **1. Morphology comparison.** For this, we will

consider the geometric microstructure models as graphs of vertices and edges, and employ approximate graph matching (often called “attributed graph matching”) algorithms (e.g., [28, 64]) to align the models being compared. Then, we will treat the morphometry (diameter, in-degree and out-degree, volume, length, etc.) associated with the pairs of vertices and edges as joint events, from which we can calculate the probability distributions. **2. Imaging comparison.** Given reconstruction \hat{M} from KESM images I , calculate $g \circ f(\hat{M})$ to regenerate an estimate of the image stack. This reconstructed volume will be directly compared with the digital phantom of manually labeled ground truth ($= g \circ f(\hat{M}_e)$). In addition, we can compare our reconstruction directly with the original KESM stack of images.

C.4.2. Conduct large-scale validation using model-based synthetic data

There is a need to scale the validation process to larger volumes of data. Several of the structures we are dealing with span very large extents in the volumetric data set (beyond the level that can be kept in memory at one time), and we must be able to reconstruct such structures. At the same time, the size of data we are dealing with makes manual reconstruction far too time-consuming. A different mode of validation is necessary.

We propose to address this scaling issue through two approaches. First, we can expand on the imaging comparison (see §C.4.1), by comparing directly to the KESM stack. The process should be the same as for smaller data sets, though it is likely that the image comparison metrics might need to change to account for variations across larger scales. Second, we will make use of synthetic data sets, which we discuss briefly below. The synthetic data sets will allow us to describe features of the reconstructed geometry at a higher level of abstraction, and ensure that we are reconstructing the overall features of microstructures, and not just the low-level geometry.

With small but accurate manually labeled ground truth reconstructions and a reliable digital phantom generator in hand, we can conduct a large-scale validation with the model-based stochastically generated data volume. The intention here is (as is often done on a smaller scale) to generate synthetic data for which we know “true” results, and confirm whether our reconstruction accurately determines the structure. We will generate multi-scale models of the vascular network using the modeling technique proposed in §C.3, generate digital phantoms from them, and conduct validation of our automated reconstruction algorithm (§C.2). See Fig. 10 for preliminary results with digital phantoms and selective manual validation.

Research issues: Generating a realistic digital phantom from the synthetic vascular network (§C.3) could be a challenge. In our previous study, we characterized the various sources of noise in KESM images [32]. We will use the noise model developed in our previous work to generate real-

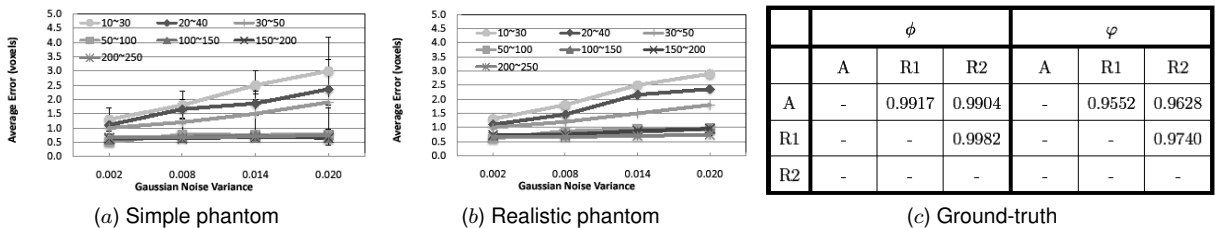


Figure 10: Pilot Validation Results. Systematic validation results with varying image contrast and noise level for digital phantoms made of (a) simple, geometric structures and (b) realistic vascular trees are shown. (c) Validation result A against two manual tracing R1 and R2 on real vascular data are shown (ϕ means length difference, and φ means centerline deviation. Values in the table are the correlation coefficients. Note that the results are very similar between *a* and *b* that use different types of phantoms, and tracing is close to perfect as can be seen in *c*. (Pilot results presented in [35].)

istic digital phantoms. Another potential issue is the disagreement among manual reconstruction. To overcome this issue, we will adopt the simultaneous truth and performance level estimation (STAPLE) approach by Commowick and Warfield [25].

C.5. Develop an SVG-based web informatics platform

To maximize the potential and impact of our whole-brain vasculature data from KESM and the validated geometric reconstructions from the data, we will develop a web-based informatics platform. We have already developed and deployed the KESM Brain Atlas, a web-based light-weight data browser for KESM mouse brain data sets, where the main innovation was the transparent overlay feature for 3D visualization [24]. The shortcoming of the previous version was that it only served raw data in raster graphics format (Portable Network Graphics, or PNG), thus geometric, quantitative data were not readily available. Also, the old version was implemented on top of Google Maps API, a proprietary API, thus limiting open-ended innovation. As part of this project, we propose to develop a Scalable Vector Graphics(SVG)-based atlas that runs on the OpenLayers API, an open-source mapping API [70]. The new informatics platform will include geometric reconstructions from §C.2 and morphometric data such as diameter, segment/element length, surface area, volume, number of branches, and order (similar to Table 3: pilot data [53]). Fig. 11 shows our prototype implementation and initial performance comparison [82]. Another key feature we will include in the proposed system is a WebGL-based interactive volume viewer integrated into the web browser. Finally, we will implement a querying system that can search and selectively show vessel segments that meet a certain search criterion (morphometry, region, topology, etc.), and generate statistical summary reports to help quantitative investigations of the data sets.

Table 2: KESM Brian Atlas Comparison.

| Version | API | Image format | Geometric Reconstruction | Speed | Morphometry | Interactive volume viewer |
|----------|-------------|--------------|--------------------------|----------------------|-------------|---------------------------|
| Previous | Google Maps | Raster (PNG) | None | Slow ($1\times$) | None | None |
| Proposed | OpenLayers | Vector (SVG) | Included | Fast (4-5 \times) | Included | WebGL-based |

Table 3: Sample Statistics from Reconstructed KESM Vasculature Data (pilot results [53]; 1 mm³).

| Region | Segments | Length (mm) | Branches | Surface (mm ²) | Volume (mm ³) | Volume (% of total) |
|-------------|----------|-------------|----------|----------------------------|---------------------------|---------------------|
| Neocortex | 11459.7 | 758.5 | 9100.0 | 10.40 | 0.0140 | 1.4% |
| Cerebellum | 34911.3 | 1676.4 | 19034.4 | 20.0 | 0.0252 | 2.5% |
| Spinal Cord | 36791.7 | 1927.6 | 26449.1 | 22.2 | 0.0236 | 2.4% |

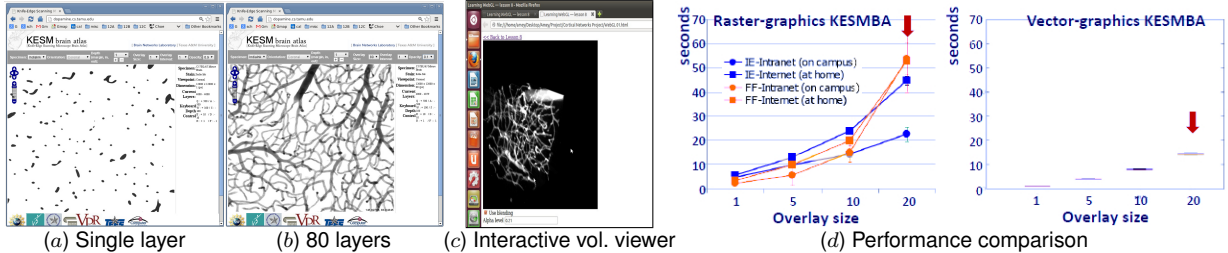


Figure 11: **SVG-based KESM Brain Atlas Prototype and Performance.** Screenshots of the SVG-based KESM Brain Atlas prototype and its performance compared to the PNG-based version are shown (pilot results from [82]). (a) A single layer at full resolution (1 μm -thick section) reveals little information. (b) An overlay of 80 images (80 μm -thick slab) shows the intricate vascular network. (c) A WebGL-based interactive volume viewer. Note that the volume is rotated away from its usual axial view, which is not possible with the overlaying technique in a–b. (d) Performance comparison of PNG-based (Left) and SVG-based (Right) KESM Brain Atlas. The SVG-based version is 4 to 5 times faster (red arrows).

Research issues: Searching with a certain geometric criterion is expected to be easy, but extraction of topological data can be hard. For example, searching for a specific “motif” (e.g., a loop) [68] is basically a subgraph isomorphism problem and it is known to be NP-complete [86]. We will adopt an index-based heuristic algorithm by Tian et al. ([83]) to overcome this issue. Finally, organizational principles and thus morphometric statistics may vary depending on the scale. We will implement support for scale-specific querying to enable investigation in this direction.

C.6. Inferring the optimization principles

The mouse brain vascular informatics platform (§C.5) opens up a unique opportunity for scientific investigation into vascular organization and development: The platform provides ample geometric and topological ground truth for structural and functional models of vascular network development: Morphometric statistics will be readily available, so various generative models of the vascular network can be easily validated.

With our informatics platform, important scientific questions can be asked, especially regarding the developmental process and optimization principles employed by the process. As we mentioned above, our vascular network data is inherently multiscale, and different developmental stages can be modeled by different scales of the data. Thus, given a generative model, we can check the morphometric distributions of not just the final result but also distributions from intermediate developmental stages. Furthermore, we can also ask important functional questions. For example, given the same functional requirements such as input blood volume, flow velocity, shear stress, pressure, and blood distribution, what type of optimization principle will lead to vascular network geometry that matches that of the observed data? Consider Fig. 12a. The four arterial trees generated by Schreiner et al. [78] were based on four different optimization criteria: total segment length, total surface, volume, and hypervolume. Our informatics platform can be used to evaluate these and other optimization criteria. As part of this project, we will compare two competing vascular network generation approaches. (1) fractal-based [5, 6] and (2) constrained constructive optimization [41, 78, 79]. We will especially focus on different developmental stages and different optimization criteria.

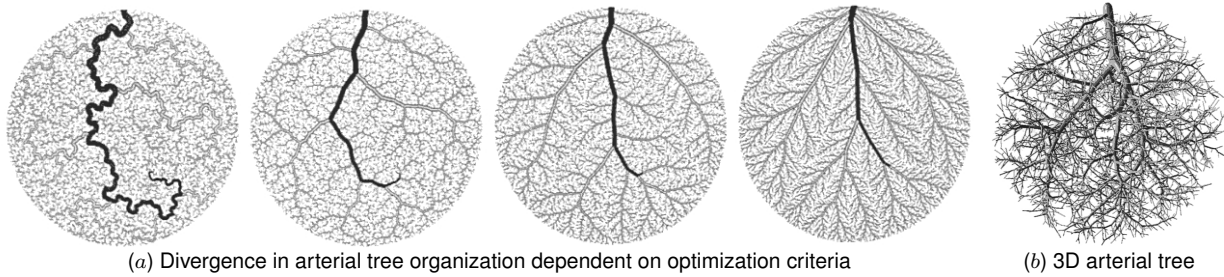


Figure 12: Constrained Constructive Optimization Model (Schreiner et al.). Results from Schreiner et al.’s Constrained Constructive Optimization Model are shown. (a) Divergence in the organization of arterial trees due to different optimization criteria is shown. From left to right, the optimization criterion was: minimum total segment length, minimum total surface, minimum volume, and minimum hypervolume. The dark marked path show the path to the same geometrical target location. (b) The algorithm can also generate data in 3D. Adapted from Schreiner et al. [78].

Research issues: Karch et al. and Schreiner et al.’s works [41, 78] model the growth of arterial trees, not the full vascular network including microcirculation near the terminal segments. A possible solution is to develop an algorithm that grows the vascular tree not from the thickest trunk but backward from the scattered terminal segments. We can run the algorithm twice to match up the arteries and the veins.

D. Broader Impact Plan

D.1. Student training and under-represented groups

This project will support the training of three Ph.D. students (two directly supported, and one other supported by other funds). Our team's previous work in this area also has a strong history of involving Master's-level students (not directly funded; seven M.S. theses have come from the group) and undergraduate students (PIs Keyser and Choe have supervised thirteen undergraduates in the past 7 years) under Research Experience for Undergraduates (REU) program (REU site, #0353957, #0649233; PI: V. E. Taylor), and the Computing Research Association(CRA)'s Distributed Research Experiences for Undergraduates (DREU) that targets under-represented groups in CS. We also received REU supplements from our current NSF grant (CRCNS) to support undergraduate research. We will continue our effort in this direction.

Our past efforts have demonstrated that we are able to incorporate under-represented groups in the project, such as women (we graduated three women in the past five years) and multiple minority students (primarily at the undergraduate level: three women [one was from an under-represented group], and two from under-represented groups). We will continue to involve and reach out to these groups in our proposed project.

D.2. Reaching out to K-12 and the general public

The resulting database and geometric reconstructions also gives us an opportunity to reach out to K-12 students and the general public. PIs Keyser and Choe have had significant experience in interactions with high-school level groups, with Keyser having given multiple presentations to such groups, and Keyser and Choe organizing a computer science contest/outreach day (hosted by the department) for high school students a total of three times in the past five years. We will organize a brain vascular network exploration contest based on simplified versions of our database and tools.

To extend our outreach beyond face-to-face interaction with the K-12 students and the public, we will leverage on our web-based informatics platform. We will engage the students and the public in two ways: (1) turn part of the reconstruction validation process into an educational game that doubles as a crowd-sourcing mechanism [87, 88], and (2) allow the students and the public to claim validated vasculature segments as their own and give them the right to name the segment. For (1), we will present the raw data overlaid with the geometric reconstruction generated from our algorithm. The user will then simply check whether the reconstruction is correct or not. For (2), given a specific vascular segment, we will take multiple user votes and pool the results (for quality control). Those who participated in that specific segment's validation will be given a chance to name the segment on a first-come first-served basis.

Seung and Burnes recently launched EyeWire, a crowd-sourcing site for tracing neuronal morphology [81]. However, the tracing task is non-trivial and may require high levels of expertise, ruling out the general public as potential users/contributors. By focusing on validation, we expect to lower the bar significantly (see our paper on interactive validation [90]). That, together with the incentive system ("name your segment", just like naming newly discovered astronomical objects), are expected to increase the interest and participation of our target audience.

D.3. Dissemination

For data dissemination, please refer to the Data Management Plan. We will actively advertise this new resource through various channels: mailing lists, news briefs in scientific publications (including popular science magazines), personal contact, and demos and exhibitions at scientific meetings. We will also organize short courses and workshops to expand and support the user community. For the above, co-PI Choe will depend on his extensive experience in most of the

above activities (Topographica software project <http://topographica.org>, book-related web page and promotion <http://computationalmaps.org> [66], exhibitions as part of the NIH/NIMH Human Brain Project, and a minisymposium [2008] and exhibits [2011, 2012] at the Society for Neuroscience meetings).

D.4. Benefits to the society:

The proposed method for data acquisition, geometric reconstruction, and automated model-based validation will result in a major resource for brain neuroanatomy rivaling the scope of the human genome project. The quantitative data reaped from our project can help launch a truly computational science of neuroanatomy and microcirculation in the brain.

E. Project Management

Management and Task breakdown: The responsibility of the PI and the Co-PIs and our planned time line for each task are shown in the table below. The order of appearance under the “Responsibility” column indicates primary and secondary person in charge, respectively. The work load is relatively lighter in the first year, so we requested support for only two graduate students. Years 2 and 3 are expected to become more intense, so we requested three students.

Table 4: Tasks, Timeline, and Responsibility

| Task | Year 1 | Year 2 | Year 3 | Responsibility |
|--|--------|--------|--------|----------------|
| C.1. Data acquisition & image proc./registration | — | — | — | Abbott, Choe |
| C.2. Fast, robust tracing algorithms | — | — | — | Keyser, Choe |
| C.3. Model-based vascular network generator | — | — | — | Choe, Abbott |
| C.4. Model-based validation | — | — | — | Keyser, Choe |
| C.5. SVG-based web informatics platform | — | — | — | Choe, Keyser |
| C.6. Inferring optimality principles | — | — | — | Abbott, Choe |
| D.2. K-12 and general public outreach | — | — | — | Choe, Keyser |
| D.3. Dissemination | — | — | — | Choe, Keyser |

Sustainability: In order to ensure continued support of the informatics platform developed through this project, we will design and implement a protocol for software development, documentation, and education. All members of the development team (both internal and external) will be trained to abide by this protocol. Involvement of external developers as well as department-funded graduate students will ensure continued support beyond the funding period. We expect maintenance to require less effort once the initial platform is implemented during the project period, and we believe we can build on the work of our recently funded CRCNS data sharing project to make dissemination easier. We will also seek continued funding from follow-up grants and from collaborations.

Broader application of our informatics framework: The rapid tracing and reconstruction algorithms and the validation framework developed in this project are expected to be applicable to other high-throughput microscopy methods. Chatter in the cutting process is common to all physical sectioning approaches involving a microtome, including Array Tomography, SBF-SEM, and ATLUM, thus the modeling framework we propose here will have a general utility beyond this project.

Summary

This project will develop an informatics platform based on fully reconstructed Knife-Edge Scanning Microscope mouse brain vascular network data. The new informatics platform and the data will enable detailed quantitative investigation of the entire vascular system in the mouse brain. The platform will be made public for scientific research and education.

REFERENCES CITED

- [1] Abbott, L. C., and Sotelo, C. (2000). Ultrastructural analysis of catecholaminergic innervation in weaver and normal mouse cerebellar cortices. *Journal of Comparative Neurology*, 426:316–329.
- [2] Al-Kofahi, K. A., Lasek, S., Szarowski, D. H., Pace, C. J., Nagy, G., Turner, J. N., and Roysam, B. (2002). Rapid automated three-dimensional tracing of neurons from confocal image stacks. *IEEE Transactions on Information Technology in Biomedicine*, 6:171–187.
- [3] Anderson, A. R. A., and Chaplain, M. A. J. (1998). Continuous and discrete mathematical models of tumor-induced angiogenesis. *Bulletin of Mathematical Biology*, 60:857–900.
- [4] Barabási, A.-L. (2002). *Linked*. Cambridge, MA: Perseus Publishing.
- [5] Bassingthwaigte, J. B., King, R. B., and Roger, S. A. (1989). Fractal nature of regional myocardial blood flow heterogeneity. *Circulation Research*, 65:578–590.
- [6] Beard, D. A., and Bassingthwaigte, J. B. (2000). The fractal nature of myocardial blood flow emerges from a whole-organ model of arterial network. *Journal of Vascular Research*, 37:282–296.
- [7] Beck Jr., L., and D’Amore, P. A. (1997). Vascular development: Cellular and molecular regulation. *The FASEB Journal*, 11:365–373.
- [8] Biggers, K., and Keyser, J. (2012). Inference-based procedural modeling of solids. *Computer Aided Design*, 18:1255–1267.
- [9] Biggers, K., Keyser, J., and Wall, J. (2010). Inference-based generative modeling of complex cluttered environments. In *Proceedings of the Interservice/Industry Training, Simulation, and Education Conference*, 2174–2184.
- [10] Blinder, P., Shih, A. Y., Rafie, C., and Kleinfeld, D. (2010). Topological basis for the robust distribution of blood to rodent neocortex. *Proceedings of the National Academy of Sciences, USA*, 28:12670–12675.
- [11] Boas, D. A., Jones, S. R., Devor, A., Huppert, T. J., and Dale, A. M. (2008). A vascular anatomical network model of the spatio-temporal response to brain activation. *NeuroImage*, 40:1116–1129.
- [12] Boldak, C., Rolland, Y., and Toumoulin, C. (2003). An improved model-based vessel tracking algorithm with application to computed tomography angiography. *Journal of Biocybernetics and Biomedical Engineering*, 3:41–64.
- [13] Braitenberg, V., and Schuz, A. (1998). *Cortex: Statistics and Geometry of Neuronal Connectivity*. Berlin: Springer. Second edition.
- [14] Brown, W. R., Blair, R. M., Moody, D. M., Thore, C. R., Ahmed, S., Robbins, M. E., and Wheeler, K. T. (2007). Capillary loss precedes the cognitive impairment induced by fractionated whole-brain irradiation: A potential rat model of vascular dementia. *Journal of the Neurological Sciences*, 257:67–71.

- [15] Can, A., Shen, H., Turner, J. N., Tanenbaum, H. L., and Roysam, B. (1999). Rapid automated tracing and feature extraction from retinal fundus images using direct exploratory algorithms. *IEEE Transactions on Information Technology in Biomedicine*, 3:125–138.
- [16] Cassot, F., Lauwers, F., Fouard, C., Prohaska, S., and Lauwers-Cances, V. (2006). A novel three-dimensional computer-assisted method for a quantitative study of microvascular networks of the human cerebral cortex. *Microcirculation*, 13:1–18.
- [17] Cassot, F., Lauwers, F., Lorthois, S., Puwanarajah, P., Cances-Lauwers, V., and Duvernoy, H. (2010). Branching patterns for arterioles and venules of the human cerebral cortex. *Brain Research*, 1313:62–78.
- [18] Choe, Y., Abbott, L. C., Han, D., Huang, P.-S., Keyser, J., Kwon, J., Mayerich, D., Melek, Z., and McCormick, B. H. (2008). Knife-edge scanning microscopy: High-throughput imaging and analysis of massive volumes of biological microstructures. In Rao, A. R., and Cecchi, G., editors, *High-Throughput Image Reconstruction and Analysis: Intelligent Microscopy Applications*, 11–37. Boston, MA: Artech House.
- [19] Choe, Y., Abbott, L. C., Miller, D. E., Han, D., Yang, H.-F., Chung, J. R., Sung, C., Mayerich, D., Kwon, J., Micheva, K., and Smith, S. J. (2010). Multiscale imaging, analysis, and integration of mouse brain networks. In *Neuroscience Meeting Planner, San Diego, CA: Society for Neuroscience*. Program No. 516.3. Online.
- [20] Choe, Y., Abbott, L. C., Ponte, G., Keyser, J., Kwon, J., Mayerich, D., Miller, D., Han, D., Grimaldi, A. M., Fiorito, G., Edelman, D. B., and McKinstry, J. L. (2010). Charting out the octopus connectome at submicron resolution using the knife-edge scanning microscope. *BMC Neuroscience*, 11(Suppl 1):P136. Nineteenth Annual Computational Neuroscience Meeting: CNS*2010.
- [21] Choe, Y., Han, D., Huang, P.-S., Keyser, J., Kwon, J., Mayerich, D., and Abbott, L. C. (2009). Complete submicrometer scans of mouse brain microstructure: Neurons and vasculatures. In *Neuroscience Meeting Planner, Chicago, IL: Society for Neuroscience*. Program No. 389.10. Online.
- [22] Choe, Y., Mayerich, D., Kwon, J., Miller, D. E., Chung, J. R., Sung, C., Keyser, J., and Abbott, L. C. (2011). Knife-edge scanning microscopy for connectomics research. In *Proceedings of the International Joint Conference on Neural Networks*, 2258–2265. Piscataway, NJ: IEEE Press.
- [23] Choe, Y., Mayerich, D., Kwon, J., Miller, D. E., Sung, C., Chung, J. R., Huffman, T., Keyser, J., and Abbott, L. C. (2011). Specimen preparation, imaging, and analysis protocols for knife-edge scanning microscopy. *Journal of Visualized Experiments*, 58:e3248. Doi: 10.3791/3248.
- [24] Chung, J. R., Sung, C., Mayerich, D., Kwon, J., Miller, D. E., Huffman, T., Abbott, L. C., Keyser, J., and Choe, Y. (2011). Multiscale exploration of mouse brain microstructures using the knife-edge scanning microscope brain atlas. *Frontiers in Neuroinformatics*, 5:29.
- [25] Commowick, O., and Warfield, S. K. (2010). Estimation of inferential uncertainty in assessing expert segmentation performance from STAPLE. *IEEE Trans. Med. Imaging*, 29(3):771–780.

- [26] Denk, W., and Horstmann, H. (2004). Serial block-face scanning electron microscopy to reconstruct three-dimensional tissue nanostructure. *PLoS Biology*, 19:e329.
- [27] Eng, D. C.-Y., and Choe, Y. (2008). Stereo pseudo 3D rendering for web-based display of scientific volumetric data. In *Proceedings of the IEEE/EG International Symposium on Volume Graphics*.
- [28] Eshera, M. A., and Fu, K. S. (1986). An image understanding system using attributed symbolic representation and inexact graph-matching. *IEEE Transactions on Pattern Analysis and Machine Intelligence*, 8:604–618.
- [29] Frangi, A. F., Niessen, W. J., Hoogeveen, R. M., Walsum, T. V., and Viergever, M. A. (1999). Model-based quantification of 3-D magnetic resonance angiographic images. *IEEE Transactions on Medical Imaging*, 18:946–956.
- [30] Grinberg, L., Anor, T., Cheever, E., Madsen, J. R., and Karniadakis, G. E. (2009). Simulation of the human intracranial arterial tree. *Philosophical Transactions of the Royal Society of London Series A*, 367:2371–2386.
- [31] Grinberg, L., Cheever, E., Anor, T., Madsen, J. R., and Karniadakis, G. E. (2010). Modeling blood flow circulation in intracranial arterial networks: A comparative 3D/1D simulation study. *Annals of Biomedical Engineering*, 39:297–309.
- [32] Guntupalli, J. S. (2007). *Physical Sectioning in 3D Biological Microscopy*. Master's thesis, Department of Computer Science, Texas A&M University.
- [33] Hagmann, P., Kurant, M., Gigandet, X., Thiran, P., Wedeen, V. J., Meuli, R., and Thiran, J.-P. (2007). Mapping human whole-brain structural networks with diffusion MRI. *PLoS ONE*, 2:e597.
- [34] Han, D. (2009). *Rapid 3D Tracing of the Mouse Brain Neurovasculature with Local Maximum Intensity Projection and Moving Windows*. PhD thesis, Department of Computer Science, Texas A&M University.
- [35] Han, D., Keyser, J., and Choe, Y. (2009). A local maximum intensity projection tracing of vasculature in Knife-Edge Scanning Microscope volume data. In *Proceedings of the IEEE International Symposium on Biomedical Imaging*, 1259–1262.
- [36] Hayworth, K. (2008). Automated creation and SEM imaging of Ultrathin Section Libraries: Tools for large volume neural circuit reconstruction. In *Society for Neuroscience Abstracts*. Washington, DC: Society for Neuroscience. Program No. 504.4.
- [37] Hayworth, K., and Lichtman, J. W. Automatic Tape-Collecting Lathe Ultramicrotome (ATLUM), http://www.mcb.harvard.edu/lichtman/ATLUM/ATLUM_web.htm.
- [38] Huang, R., Melek, Z., and Keyser, J. (2011). Preview-based sampling for controlling gaseous simulations. In *Proceedings of Symposium on Computer Animation*, 177–186.
- [39] Jacobowitz, D. M., and Abbott, L. C. (1997). *Chemoarchitectonic Atlas of the Developing Mouse Brain*. Boca Raton, FL: CRC Press.
- [40] Jacobs, R. E., Ahrens, E. T., Dickinson, M. E., and Laidlaw, D. (1999). Towards a microMRI atlas of mouse development. *Computerized Medical Imaging and Graphics*, 23:15–24.

- [41] Karch, R., Neumann, R., Neumann, M., and Schreiner, W. (2000). Staged growth of optimized arterial model trees. *Annals of Biomedical Engineering*, 28:495–511.
- [42] Kaufhold, J. P., Tsai, P. S., Blinder, P., and Kleinfeld, D. (2012). Vectorization of optically sectioned brain microvasculature: Learning aids completion of vascular graphs by connecting gaps and deleting open-ended segments. *Medical Image Analysis*, 16:1241–1258.
- [43] Khan, M. A. U., Truc, P. T. H., Bahadur, R., and Javed, S. (2007). Vessel enhancement using directional features. *Information Technology Journal*, 6:851–857.
- [44] Kwon, J., Mayerich, D., and Choe, Y. (2011). Automated cropping and artifact removal for knife-edge scanning microscopy. In *Proceedings of the IEEE International Symposium on Biomedical Imaging*, 1366–1369.
- [45] Kwon, J., Mayerich, D., Choe, Y., and McCormick, B. H. (2008). Lateral sectioning for knife-edge scanning microscopy. In *Proceedings of the IEEE International Symposium on Biomedical Imaging*, 1371–1374.
- [46] Kwon, J.-R. (2009). *Acquisition and Mining of the Whole Mouse Brain Microstructure*. PhD thesis, Department of Computer Science, Texas A&M University.
- [47] Lawson, N. D., and Weinstein, B. M. (2002). In Vivo imaging of embryonic vascular development using transgenic zebrafish. *Developmental Biology*, 248:307–318.
- [48] Lee, J. H., Terashima, M., Seo, W. S., Kosuge, H., Sherlock, S., McConnel, M., Nishimura, D., and Daiv, H. (2008). 2119 visualization of micro-vasculature using FeCo-core/graphite-carbon-shell nanocrystals and high-resolution 3D spiral imaging. *Journal of Cardiovascular Magnetic Resonance*, 10(Suppl 1):A388.
- [49] Li, A., Gong, H., Zhang, B., Wang, Q., Wan, C., Wu, J., Liu, Q., Zeng, S., and Luo, Q. (2010). Micro-optical sectioning tomography to obtain a high-resolution atlas of the mouse brain. *Science*. In press.
- [50] Mayerich, D., Abbott, L. C., and Keyser, J. (2008). Visualization of cellular and microvessel relationship. *IEEE Transactions on Visualization and Computer Graphics (Proceedings of IEEE Visualization)*, 14:1611–1618.
- [51] Mayerich, D., Abbott, L. C., and McCormick, B. H. (2008). Knife-edge scanning microscopy for imaging and reconstruction of three-dimensional anatomical structures of the mouse brain. *Journal of Microscopy*, 231:134–143.
- [52] Mayerich, D., and Keyser, J. (2008). Filament tracking and encoding for complex biological networks. In *Proceedings of ACM Symposium on Solid and Physical Modeling*, 353–358.
- [53] Mayerich, D., Kwon, J., Choe, Y., Abbott, L., and Keyser, J. (2008). Constructing high-resolution microvascular models. In *Proceedings of the 3rd International Workshop on Microscopic Image Analysis with Applications in Biology (MIAAB 2008)*. Online.
- [54] Mayerich, D., Kwon, J., Panchal, A., Keyser, J., and Choe, Y. (2011). Fast cell detection in high-throughput imagery using gpu-accelerated machine learning. In *Proceedings of the IEEE International Symposium on Biomedical Imaging*, 719–723.

- [55] Mayerich, D., Kwon, J., Sung, C., Abbott, L. C., Keyser, J., and Choe, Y. (2011). Fast macro-scale transmission imaging of microvascular networks using KESM. *Biomedical Optics Express*, 2:2888–2896.
- [56] Mayerich, D., McCormick, B. H., and Keyser, J. (2007). Noise and artifact removal in knife-edge scanning microscopy. In *Proceedings of the IEEE International Symposium on Biomedical Imaging*, 556–559.
- [57] Mayerich, D. M., and Keyser, J. (2008). Filament tracking and encoding for complex biological networks. In *Proceedings of Solid Modeling*. To appear.
- [58] McCormick, B. H. (2003). The knife-edge scanning microscope. Technical report, Department of Computer Science, Texas A&M University. <http://research.cs.tamu.edu/bnl/>.
- [59] McCormick, B. H., System and method for imaging an object. USPTO patent #US 6,744,572 (for Knife-Edge Scanning; 13 claims).
- [60] McCormick, B. H., Abbott, L. C., Mayerich, D. M., , Keyser, J., Kwon, J., Melek, Z., and Choe, Y. (2006). Full-scale submicron neuroanatomy of the mouse brain. In *Society for Neuroscience Abstracts*. Washington, DC: Society for Neuroscience. Program No. 694.5. Online.
- [61] McCormick, B. H., and Mayerich, D. M. (2004). Three-dimensional imaging using Knife-Edge Scanning Microscope. *Microscopy and Microanalysis*, 10 (Suppl. 2):1466–1467.
- [62] McLachlan, G. J., and Krishnan, T. (1996). *The EM Algorithm and Extensions*. John Wiley and Sons.
- [63] Melek, Z., Mayerich, D., Yuksel, C., and Keyser, J. (2006). Visualization of fibrous and thread-like data. *IEEE Transactions on Visualization and Computer Graphics*, 12(5):1165–1172.
- [64] Melnik, S., Garcia-Molina, H., and Rahm, E. (2002). Similarity flooding: A versatile graph matching algorithm and its application to schema matching. In *Proceedings of the 18th International Conference on Data Engineering*, 117–128.
- [65] Micheva, K., and Smith, S. J. (2007). Array tomography: A new tool for imaging the molecular architecture and ultrastructure of neural circuits. *Neuron*, 55:25–36.
- [66] Miikkulainen, R., Bednar, J. A., Choe, Y., and Sirosh, J. (2005). *Computational Maps in the Visual Cortex*. Berlin: Springer. URL: <http://www.computationalmaps.org>.
- [67] Miller, J. S., Stevens, K. R., Yang, M. T., Baker, B. M., Nguyen, D. T., Chen, A. A., Galie, P. A., Yu, X., Chaturvedi, R., Bhatia, S. N., and Chen, C. S. (2012). Rapid casting of patterned vascular networks for perfusable engineered three-dimensional tissues. *Nature Materials*, 11:768–774.
- [68] Milo, R., Shen-Orr, S., Itzkovitz, S., Kashtan, N., Chklovskii, D., and Alon, U. (2002). Network motifs: Simple building blocks of complex networks. *Science*, 298:824–827.
- [69] Nakagami, H., Nakagawa, N., Takeya, Y., Kashiwagi, K., Ishida, C., ichiro Hayashi, S., Aoki, M., Matsumoto, K., Nakamura, T., Ogihara, T., and Morishita, R. (2006). Model of vasculogenesis from embryonic stem cells for vascular research and regenerative medicine. *Hypertension*, 48:112–119.

- [70] Open Source Geospatial Foundation, Openlayers version 2.12. <http://openlayers.org/>.
- [71] Pham, D. L., Xu, C., and Prince, J. L. (2000). Current methods in medical image segmentation. *Annual Review of Biomedical Engineering*, 2:315–337.
- [72] Plouraboué, F., Cloetens, P., Fonta, C., Steyer, A., Lauwers, F., and Marc-Vergnes, J.-P. (2004). X-ray high-resolution vascular network imaging. *Journal of Microscopy*, 215:139–148.
- [73] Pluim, J. P. W., Maintz, J. B. A., and Viergever, M. A. (2000). Image registration by maximization of combined mutual information and gradient information. In *Lecture Notes In Computer Science, Vol. 1935; Proceedings of the Third International Conference on Medical Image Computing and Computer-Assisted Intervention*, 452–461. London: Springer.
- [74] Ragan, T., Kadiri, L. R., Venkataram, K. U., Bahlmann, K., Sutin, J., Taranda, J., Arganda-Carreras, I., Kim, Y., Seung, H. S., and Osten, P. (2012). Serial two-photon tomography for automated *ex vivo* mouse brain imaging. *Nature Methods*, 9:255–258.
- [75] Rhyu, I. J., and D. B. Walker, L. C. A., and Sotelo, C. (1999). An ultrastructural study of granule cell/Purkinje cell synapses in tottering (tg/tg), leaner (tg^{la}/tg^{la}) and compound heterozygous tottering/leaner (tg/tg^{la}) mice. *Neuroscience*, 90:717–728.
- [76] Rosenblum, W. I., and Zweifach, B. W. (1963). Cerebral microcirculation in the mouse brain: Spontaneous and drug-induced changes in flow and vascular diameter. *Archives of Neurology*, 9:414–423.
- [77] Schaefer, S., McPhail, T., and Warren, J. (2006). Image deformation using moving least squares. *ACM Transactions on Graphics*, 25(3):533–540.
- [78] Schreiner, W., Karch, R., Neumann, F., and Neumann, M. (2000). Constrained constructive optimization of arterial tree models. In Brown, J. H., and West, G. B., editors, *Scaling in Biology*, 145–165. Oxford, UK: Oxford University Press.
- [79] Schreiner, W., Karch, R., Neumann, M., Neumann, F., Szawlowski, P., and Roedler, S. (2006). Optimized arterial trees supplying hollow organs. *Medical Engineering & Physics*, 28:416–429.
- [80] Serini, G., Ambrosi, D., Giraudo, E., Gamba, A., Preziosi, L., and Bussolino, F. (2003). Modeling the early stages of vascular network assembly. *The EMBO Journal*, 22:1771–1779.
- [81] Seung, S., and Burnes, L., Eyewire. <http://eyewire.org/>.
- [82] Sung, C., Mayerich, D., Kwon, J., Miller, D. E., Abbott, L. C., Keyser, J., Huffman, T., and Choe, Y. (2011). Web-based knife-edge scanning microscope brain atlas in vector-graphics for enhanced performance. In *Neuroscience Meeting Planner, New Orleans, LA: Society for Neuroscience*. Program No. 328.05. Online.
- [83] Tian, Y., McEachin, R. C., Santos, C., States, D. J., and Patel, J. M. (2007). SAGA: A subgraph matching tool for biological graphs. *Bioinformatics*, 23:232–239.
- [84] Tong, S., and Yuan, F. (2001). Numerical simulations of angiogenesis in the cornea. *Microvascular Research*, 61:14–27.

- [85] Tsai, P. S., Friedman, B., Ifarraguerri, A. I., Thompson, B. D., Lev-Ram, V., Schaffer, C. B., Xiong, Q., Tsien, R. Y., Squier, J. A., and Kleinfeld, D. (2003). All-optical histology using ultrashort laser pulses. *Neuron*, 39:27–41.
- [86] Ullmann, J. R. (1976). An algorithm for subgraph isomorphism. *Journal of the ACM*, 23:31–41.
- [87] von Ahn, L., Kedia, M., and Blum, M. (2006). Peekaboom: A game for locating objects in images. In *Proceedings of the ACM Conference on Human Factors in Computing Systems (CHI 2006)*, 55–64.
- [88] von Ahn, L., Maurer, B., McMillen, C., Abraham, D., and Blum, M. (2008). reCAPTCHA: Human-based character recognition via web security measures. *Science*, 321:1465–1468.
- [89] Warfield, S. J., Zou, K. H., and Wells, W. M. (2002). Validation of image segmentation and expert quality with expectation-minimization algorithm. In *Lecture Notes In Computer Science, Vol. 2488; Proceedings of the 5th International Conference on Medical Image Computing and Computer-Assisted Intervention*, 298–306.
- [90] Yang, H.-F., and Choe, Y. (2011). An interactive editing framework for electron microscopy image segmentation. In *Proceedings of the 7th International Symposium on Visual Computing (LNCS 6938)*, 400–409.
- [91] Yoo, T., Ackerman, N. J., and Vannier, M. (2000). Toward a common validation methodology for segmentation and registration algorithms. In *Lecture Notes In Computer Science, Vol. 1935; Proceedings of the Third International Conference on Medical Image Computing and Computer-Assisted Intervention*, 422–431. London: Springer.
- [92] Yuksel, C., Schaefer, S., and Keyser, J. (2011). Parameterization and applications of catmull-rom curves. *Computer Aided Design*, 43:747–755.